Nasally delivered VEGFD mimetics mitigate stroke-induced dendrite loss and brain damage

Daniela Mauceri[a], Bettina Buchthal[a], Thekla J. Hemstedt[a], Ursula Weiss[a], Christian D. Klein[b], and Hilmar Bading[a,1]

[a]Department of Neurobiology, Interdisciplinary Center for Neurosciences (IZN), Heidelberg University, Im Neuenheimer Feld (INF) 366, 69120 Heidelberg, Germany; and [b]Medicinal Chemistry, Institute of Pharmacy and Molecular Biotechnology, Heidelberg University, INF 364, 69120 Heidelberg, Germany

Edited by Michael E. Greenberg, Harvard Medical School, Boston, MA, and approved March 3, 2020 (received for review January 31, 2020)

In the adult brain, vascular endothelial growth factor D (VEGFD) is required for structural integrity of dendrites and cognitive abilities. Alterations of dendritic architectures are hallmarks of many neurologic disorders, including stroke-induced damage caused by toxic extrasynaptic NMDA receptor (eNMDAR) signaling. Here we show that stimulation of eNMDARs causes a rapid shutoff of *VEGFD* expression, leading to a dramatic loss of dendritic structures. Using the mouse middle cerebral artery occlusion (MCAO) stroke model, we have established the therapeutic potential of recombinant mouse VEGFD delivered intraventricularly to preserve dendritic architecture, reduce stroke-induced brain damage, and facilitate functional recovery. An easy-to-use therapeutic intervention for stroke was developed that uses a new class of VEGFD-derived peptide mimetics and postinjury nose-to-brain delivery.

dendrite | extrasynaptic NMDA receptor | nose-to-brain delivery | stroke | VEGFD

Ischemic stroke is one of the leading causes of death worldwide (1). Stroke survivors are often left struggling with severe motor impairments and/or cognitive disabilities, which represent a significant burden for patients, caregivers, and the economy. Neurons begin to die within minutes after the onset of the ischemic event; thus, restoring blood flow is paramount and is the only currently available therapeutic approach. However, the vast majority of patients are not suitable for thrombolytic therapy due to several contraindications and the narrow time window for delivery (2). Thus, there is an unmet need for additional therapeutic approaches. In addition to cell death, it has been observed that stroke destabilizes spines and dendritic connections of the surviving neurons located in the peri-infarct, adjacent brain areas (3–5).

Because neuronal connections represent the hardware for proper cognitive abilities, therapeutic strategies aimed at preserving dendritic connections could conceivably be beneficial in stroke. Here we present the prototype of a structure-protective stroke therapy based on a newly developed class of peptide mimetics derived from vascular endothelial growth factor D (VEGFD), a previously characterized key dendrite maintenance factor that is critical for cognitive functions (6–9). VEGFD is known to be enriched in nonbrain regions, most notably in endothelial cells (10). However, recent proteomics and single-cell sequencing analyses revealed considerable levels of VEGFD expression in the brain that in some cases are higher in neuronal cells than in endothelial cells (11–13). Supplementation of VEGFD peptide mimetics counteracts the stroke-associated loss of endogenous VEGFD, thereby preventing the loss of structural integrity of neurons, reducing infarct volume, and promoting functional recovery.

Results and Discussion

While expression of VEGFD is upheld by neuronal activity and calcium flux through synaptic NMDA receptors (sNMDARs) (6), we report here that stimulation of extrasynaptic NMDA receptors (eNMDARs) leads to the shutoff of VEGFD expression. eNMDARs were activated in primary hippocampal neurons by bath application of NMDA, which caused a progressive decline in *VEGFD* mRNA levels (Fig. 1*A*). The shutoff of VEGFD was NMDA concentration-dependent (*SI Appendix*, Fig. S1*A*), triggered within minutes of NMDA application (*SI Appendix*, Fig. S1*B*) and was not due to a change in the stability of *VEGFD* mRNA (*SI Appendix*, Fig. S1*C*). The NMDA-induced shutoff was selective for VEGFD, inasmuch as several other genes were not reduced. This includes the immediate early gene c*Fos*, other members of the VEGF family (i.e., *VEGFC*, *VEGF*), and the VEGFD receptor *flt4*/*VEGFR3* (*SI Appendix*, Fig. S1 *D* and *E*).

Because NMDA bath application also stimulates synaptic NMDARs (sNMDARs), we used a bicuculline/MK-801 pretreatment to pharmacologically isolate eNMDARs. This protocol makes use of the fact that MK-801, an open-channel NMDAR antagonist, blocks only sNMDARs in cultured hippocampal neurons that undergo bursts of action potential firing triggered by the GABAA receptor antagonist bicuculline (14, 15). After washout of bicuculline/MK-801 and silencing of synaptic activity using TTX, eNMDARs can be stimulated by bath application of NMDA (14, 15). The bicuculline/MK-801 protocol confirmed that eNMDARs are responsible for the shutoff of VEGFD expression (Fig. 1*B*). In contrast, stimulation of sNMDARs evoked by bicuculline treatment in the presence of the potassium channel blocker 4-aminopyridine

Significance

Stroke is a leading cause of death worldwide. Survivors generally suffer severe disabilities. The sole currently available therapy, which restores impaired blood flow, has many contraindications. Using in vitro and in vivo stroke models, we show that stimulation of extrasynaptic NMDA receptors shuts off *Vascular Endothelial Growth Factor D* (*VEGFD*) expression, causing loss of dendrites. Intraventricular administration of recombinant VEGFD to mice suffering a stroke preserves dendritic architecture, reduces brain damage, and facilitates functional recovery. Similarly, VEGFD mimetics applied nasally prevents stroke-induced damage. Thus, a new neuroprotective approach has been established that preserves neuronal structural integrity through supplementation of VEGFD. It can serve as standalone therapy or complementary medicine to existing treatments of nervous system disorders with structural impairments.

Author contributions: D.M. and H.B. designed research; D.M., B.B., T.J.H., and U.W. performed research; C.D.K. contributed new reagents/analytic tools; D.M., B.B., T.J.H., and U.W. analyzed data; C.D.K. designed the peptides used for screening; and D.M. and H.B. wrote the paper.

Competing interest statement: D.M. and H.B. are founders and shareholders of Fundamental Pharma GmbH, which licenses the FMP peptides. H.B., D.M., and C.D.K. are inventors of the relative patent (USA: US9415090; Canada: CA283483; European Office: EP2714063).

This article is a PNAS Direct Submission.

Data deposition: All data shown in the paper have been deposited in Figshare, https://doi.org/10.6084/m9.figshare.11920116.

[1]To whom correspondence may be addressed. Email: bading@nbio.uni-heidelberg.de.

This article contains supporting information online at https://www.pnas.org/lookup/suppl/doi:10.1073/pnas.2001563117/-/DCSupplemental.

First published March 30, 2020.

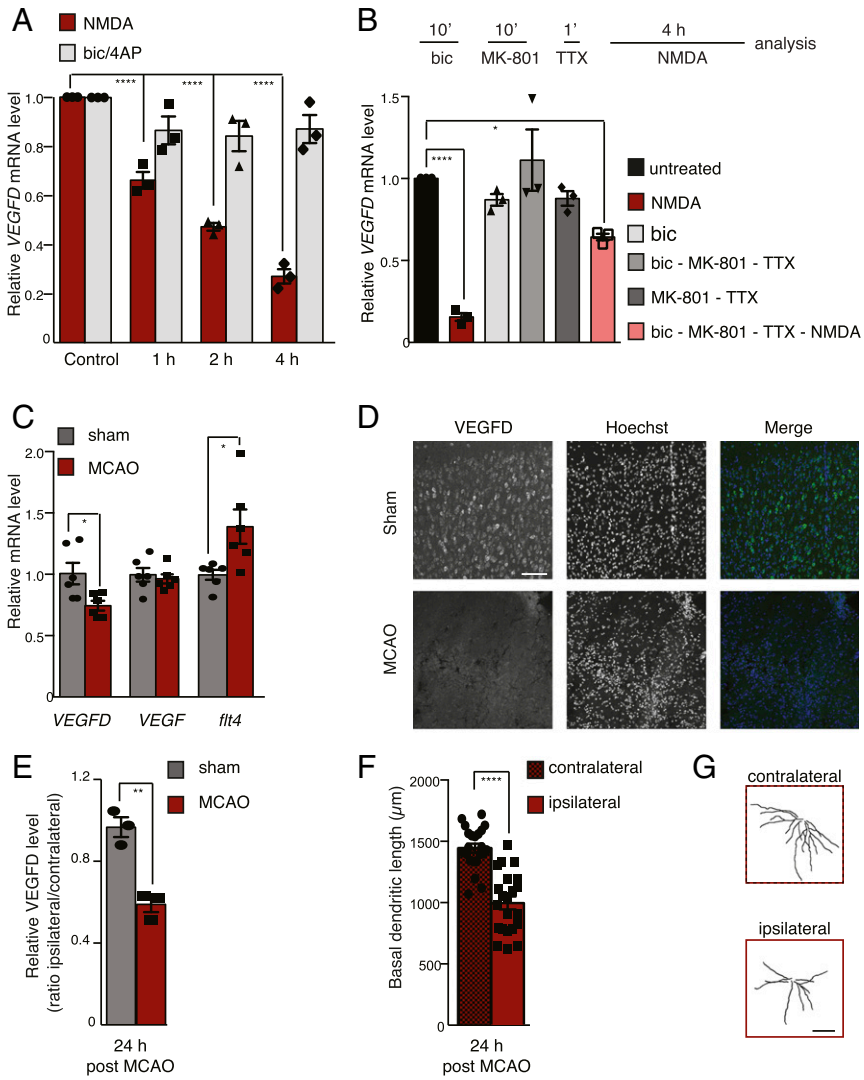

Fig. 1. eNMDARs activation causes VEGFD shut-off in vitro and in vivo. (*A*) qRT-PCR analysis of *VEGFD* expression in cultured hippocampal neurons with or without treatment of 50 μM bicuculline/250 μM 4-amino pyridine (Bic/4AP) or 20 μM NMDA for the indicated times ($n = 3$). (*B*) qRT-PCR analysis of *VEGFD* expression in cultured hippocampal neurons after the indicated treatments $n = 3$. (*C*) qRT-PCR analysis of *VEGFD, VEGF*, and *flt4* expression in ipsilateral cortex of mice MCAO or sham at 24 h after surgery. $n = 6$. (*D*) Representative images of the ipsilateral cortices of adult mice after MCAO or sham surgery. Coronal sections were immunolabeled for VEGFD (green); nuclei were labeled with Hoechst (blue). (Scale bar: 100 μm.) (*E*) Quantification of VEGFD protein levels in ipsilateral cortex of mice after MCAO or sham surgery as indicated ($n = 3$). (*F*) Basal dendritic length of layer 2/3 pyramidal neurons from the ipsilateral and contralateral cortices of mice at 24 h after MCAO ($n = 22$ neurons, 4 mice). (*G*) Representative tracings of the basal dendritic trees of neurons analyzed as in *F*. (Scale bar: 50 μm.) *A* and *B*, one-way ANOVA with Dunnett's correction for multiple comparisons; *C*, *E*, and *F*, unpaired *t* test. $^*P < 0.05$; $^{***}P < 0.001$; $^{****}P < 0.0001$. Plotted data show mean ± SEM and individual values.

(4AP) to increase the burst frequencies for 1 to 4 h had no effect on *VEGFD* mRNA levels (Fig. 1*A* and *SI Appendix*, Fig. S1*D*).

Heightened eNMDAR signaling is associated with several acute and chronic neurodegenerative diseases (16–18). During a stroke, eNMDARs are being activated due to pathological increases in extracellular glutamate concentration caused by reverse operation of neuronal and glial glutamate transporters in hypoxic/ischemic conditions and glutamate release by the cystine-glutamate antiporter (19, 20). Therefore, we expected to observe a stroke-associated decline in *VEGFD* expression. Stroke can be mimicked in vitro by oxygen-glucose deprivation (OGD) of neurons (14). We found that 4 h of OGD led to a dramatic reduction of *VEGFD* mRNA levels (*SI Appendix*, Fig. S1*F*). A similar reduction was observed in vivo in the unilateral middle cerebral artery occlusion (MCAO) mouse stroke model (21, 22). *VEGFD* mRNA and protein levels in the ipsilateral cortices were significantly lower than those in sham-operated animals at 24 h after injury (Fig. 1 *C*–*E*). *VEGF* mRNA levels were analyzed in parallel and were found unaltered, while *flt4* showed increased expression after MCAO, consistent with a previous report (Fig. 1*C*) (23). In the contralateral cortices as well as in the hippocampi of MCAO-treated mice, which are not affected in the MCAO model, no changes in *VEGFD* mRNA levels were detected (*SI Appendix*, Fig. S1 *G* and *H*). Moreover, NMDA bath application to cultured endothelial cells or astrocytes had no effect on *VEGFD* mRNA levels (*SI Appendix*, Fig. S1 *I* and *J*), indicating that the observed VEGFD reduction may take place primarily in neuronal cells. Thus, stroke is associated with the shutoff of VEGFD, the consequence of which may be a loss of structural integrity of neurons.

It is well established that cerebral ischemia can lead to structural alteration of neurons, which includes simplification but also sprouting of dendritic trees (5, 24, 25). Therefore, we analyzed

layer 2/3 cortical pyramidal neurons located in the penumbra area of the ipsilateral cortex and found a shorter total length of basal dendrites compared with neurons of the contralateral cortex at 24 h after MCAO (Fig. 1 *F* and *G*). Thus, the observed loss of VEGFD expression after MCAO is indeed paralleled by a loss of structural integrity of the neurons.

To establish a causal link between loss of VEGFD and structural disintegration, we rescued the loss of VEGFD by stereotactically injecting adult mice intracerebroventricularly (i.c.v.) with recombinant mouse VEGFD (rmVEGFD) or with recombinant GFP (control). Both proteins could be detected in sham-operated mice in brain areas ipsilateral to the injection side via immunoblot analysis of brain lysates prepared at 1 h and 2 h after stereotactic protein delivery (Fig. 2*A*). We observed a robust structure-protective effect on VEGFD supplementation. While mice that received a 10-min post-MCAO i.c.v. injection of GFP or saline (Fig. 2 *B–D*) showed a dramatic loss of basal dendrites of layer 2/3 pyramidal neurons on the ipsilateral site, no structural impairments of basal dendrites of layer 2/3 pyramidal neurons were observed in mice subjected to a 10 min post-MCAO i.c.v. injection of rmVEGFD (Fig. 2*D*). Thus, supplementation of VEGFD mitigates the stroke-induced loss of dendritic structure, thereby preserving the integrity of the neurons and their synaptic connectivity.

Given that neuronal survival is strongly promoted by synaptic activity (14, 26, 27), which relies on intact synaptic connections and thus also on the integrity of the dendritic arbor, we predicted that structure protection via VEGFD supplementation would preserve synaptic activity within the networks, thereby promoting survival and reducing stroke-associated brain damage. Indeed, we observed a robust improvement of stroke outcomes in terms of both brain damage and functional recovery. A 10-min post-MCAO i.c.v. injection of rmVEGFD significantly reduced the infarct volume assessed at 8 d after injury (Fig. 2 *B*, *C*, *E*, and *F*). This protective effect took place in the absence of changes of total length of visible pial surface vessels of the ipsilateral cortices and density of capillaries, visualized using fluorescein isothiocyanate-dextran perfusion, which were found to be similar between saline and rmVEGFD-treated mice at 24 h or 8 d post-MCAO (*SI Appendix*, Fig. S1 *K* and *L*). The observed therapeutic effect was specific for VEGFD, because GFP as well as recombinant VEGFC (rVEGFC) or recombinant VEGF (rVEGF) did not reduce the MCAO-induced infarct volume (Fig. 2 *G* and *H*), in agreement with the observation that VEGFC and VEGF do not possess dendritic-maintenance properties (6, 9).

In light of the lack of a direct effect of VEGFD on the survival of neurons, as shown by the absence of neuroprotective activity of VEGFD in classical in vitro cell death assays, such as NMDA toxicity or OGD (14) (Fig. 2*I*), the results obtained, including our in vitro data on VEGFD structure protective activity (Fig. 2*J*), strongly support the concept that the structure-preserving function of VEGFD underlies the therapeutic benefits of VEGFD and prevents neurons from dying. Supplementation of VEGFD preserves the structure of neurons and their synaptic connectivity within the network, thereby preventing endogenous, activity-regulated neuroprotective processes from being disabled during stroke. Our results and previous studies (6) suggest a direct mechanism of action of VEGFD on dendrites, although we cannot rule out the involvement of other cell types in the preservation of neuronal structures. The structure-preserving and brain damage-reducing effects translate into improved functional recovery. This was monitored with a corner test for 8 d post-MCAO, which revealed an accelerated functional recovery rate in rmVEGFD-injected mice compared with the saline-injected mice (Fig. 2*K*).

To improve the clinical applicability of this novel type of treatment and to make it suitable for stroke patients, we explored the possibility of nose-to-brain delivery (Fig. 3 *A* and *B*). This very simple and, most importantly, noninvasive route of administration has been used for the successful delivery of several peptides and proteins in animal models (22, 28–34) and is under investigation in clinical trials (https://clinicaltrials.gov/ct2/home). In addition, it appears that nose-to-brain delivery does not involve systemic circulation and bypasses the blood-brain barrier (35). We first established the procedure with rmVEGFD. While we obtained a very robust therapeutic effect using nasally applied rmVEGFD (see below), we were unable to detect the recombinant protein in lysates from brain tissue of mice that received rmVEGFD via nose drops.

The detection methods used included immunohistochemistry, immunoblotting, and ELISA, which most likely are not sensitive enough to detect the small amount of rmVEGFD in brain homogenates. Nevertheless, we observed robust biological effects indicative of successful rmVEGFD delivery to the brain. Mice subjected to MCAO and treated postinjury with three nasal applications of rmVEGFD showed a significant reduction in the infarct volume compared with vehicle- and GFP-treated animals (Fig. 3 *B–D*). They also displayed no detectable loss of basal dendrites in the layer 2/3 neurons ipsilateral to the MCAO compared with the contralateral side (Fig. 3 *E* and *F*) and, moreover, showed improved functional recovery post-MCAO compared with vehicle-treated mice (Fig. 3*G*).

These results suggest that nasal delivery of rmVEGFD may be suitable for stroke therapy. To further simplify the therapeutic intervention and make it more cost-effective, we developed VEGFD peptide mimetics. VEGFD maintains dendritic architecture via activation of VEGFR3, and its neuronal signaling has been previously characterized (6); the available structural data indicate that the N-terminal alpha helix of mature VEGFD mediates such interaction (36). Thus, we identified a sequence motif in VEGFD, which we expected to have agonist properties at the receptor. We generated a library of 16-aa-long peptides in which this sequence was varied in a systematic manner to identify VEGFD peptide mimetics with increased agonist activity (*SI Appendix*, Fig. S2).

Since the helical folding of the motif appears to be critical, we introduced residues and pairs of residues that increase the propensity for helical folding. Among these residues were alanine, the nonnatural amino acids alpha-amino-isobutyric acid (aib) and gabapentine, as well as pairs of cationic and anionic amino acids. We screened 96 VEGFD peptide mimetics candidates using biochemical assays of signaling events known to be triggered by VEGFD (6), in vitro measurements of dendrite-preserving activities (6), and cell toxicity (*SI Appendix*, Figs. S2 and S3). Two high-performing peptides (FMP6 and FMP69) were selected and tested for therapeutic efficacy in vivo. Both FMP6 and FMP69 delivered nasally postinjury (Fig. 4 *A* and *B*) completely protected layer 2/3 neurons from MCAO-induced structural damage of dendrites (Fig. 4 *C* and *D*), while a scrambled version of FMP6 (scrFMP6) used as a control showed no effect (Fig. 4 *E* and *F*). Moreover, postinjury nasal delivery of FMP6 and FMP69, but not of the control scrambled peptide scrFMP6, led to a strong reduction in infarct volume (Fig. 4 *G–I*). Finally, behavioral assessments using the corner test revealed that compared with vehicle or scrFMP6 controls, nasally applied FMP6 significantly improved functional recovery (Fig. 4*J*).

In conclusion, our study uncovered the eNMDAR-induced VEGFD shutoff based on which a new concept in neuroprotective therapy has been established. Preserving the structural integrity of neurons by supplementing VEGFD holds great potential to be translated into clinical application as standalone stroke therapy or as an aid to existing treatment. The combination of low-cost VEGFD peptide mimetics with an extraordinarily simple postinjury nasal delivery makes this new and presumably safe treatment an easy-to-use therapeutic intervention that could be given to stroke patients even by laypersons immediately after the insult. A similar treatment may also be effective for chronic neurodegenerative diseases, many

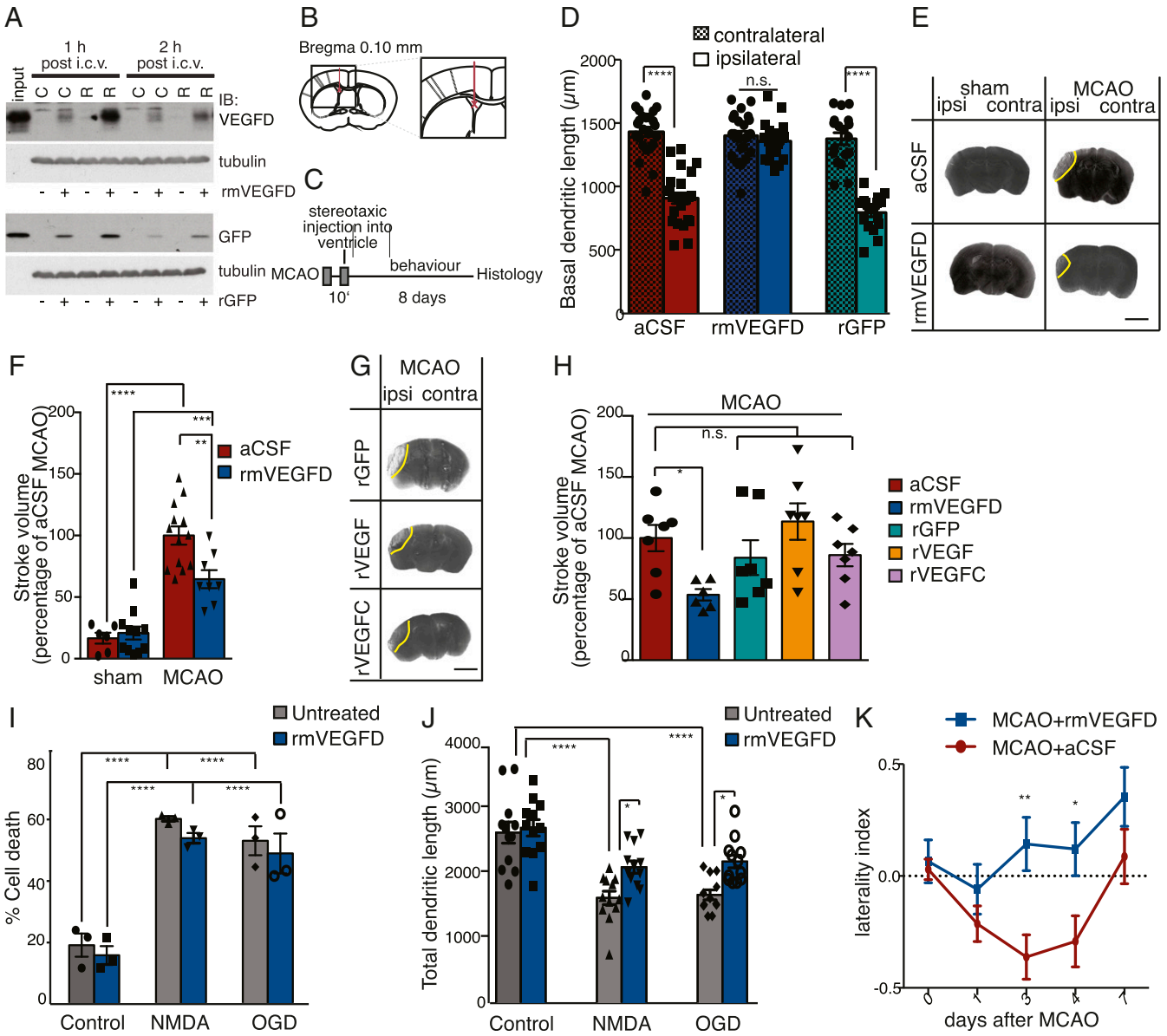

Fig. 2. Intracerebroventricular delivery of rmVEGFD counteracts MCAO-induced brain damage by preserving dendritic structure. (*A*) Immunoblot analysis of rmVEGFD and rGFP in cortex lysates (C) and in lysates containing striatum, putamen, basal forebrain, thalamus, and hypothalamus (R) collected at 1 h or 2 h post-i.c.v. injection. Input was rGFP or rmVEGFD; tubulin served as a loading control. (*B*) Schematic illustration of unilateral stereotactic i.c.v. injections into the left ventricle. (*C*) Timeframe of the experiment. Mice were injected at 10 min after MCAO, and histological analysis was performed at 8 d post-MCAO, motor recovery was assessed in the meantime. (*D*) Basal dendritic length of layer 2/3 pyramidal neurons from the ipsilateral and contralateral cortices of mice post-MCAO and i.c.v. injected with GFP, rVEGFD, or aCSF (aCSF: $n = 24$ neurons, 4 mice; rmVEGFD: $n = 23$ to 24 neurons; 4 mice; rGFP: $n = 18$ neurons, 3 mice). (*E*) Silver-stained coronal brain sections of mice after MCAO or sham surgery i.c.v. injected with rmVEGFD or aCSF. Infarcted tissue appears as lighter gray. The yellow line indicates the border of the damaged area. (Scale bar: 0.20 cm.) (*F*) Infarct volumes in brains of mice subjected to MCAO or sham surgery and i.c.v. injected as indicated. (sham: aCSF, $n = 6$, rmVEGFD, $n = 11$; MCAO: aCSF, $n = 13$, rmVEGFD, $n = 8$). (*G*) Silver-stained coronal brain sections of mice after post-MCAO i.c.v. injection as indicated. (Scale bar: 0.20 cm.) (*H*) Infarct volumes in brains of mice subjected to MCAO and i.c.v.-injected with rmVEGFD ($n = 6$), rGFP ($n = 7$), rVEGF ($n = 7$), rVEGFC ($n = 7$), or aCSF ($n = 7$). (*I*) Mortality rate of hippocampal neurons treated with NMDA or exposed to OGD for 10 min, with or without rmVEGFD, analyzed at 24 h after insult ($n = 3$). (*J*) Total dendritic length of cultured neurons as in *I* ($n = 12$). (*K*) Corner test of mice before and after MCAO and i.c.v. injection of rmVEGFD ($n = 12$) or aCSF ($n = 15$). *D*, unpaired *t* test; *F*, one-way ANOVA with Bonferroni's correction for multiple comparisons; *H*, one-way ANOVA with Dunnett's correction for multiple comparisons; *I* and *J*, one-way and two-way ANOVA with Bonferroni's correction for multiple comparisons; *K*, two-way ANOVA with Bonferroni's correction for multiple comparisons. $^*P < 0.05$; $^{**}P < 0.01$; $^{***}P < 0.001$; $^{****}P < 0.0001$. Plotted data show mean ± SEM and individual values.

of which, including amyotrophic lateral sclerosis, Huntington's disease, and Alzheimer's disease, are associated with heightened eNMDAR signaling (16) and, conceivably, with the shutdown of VEGFD expression. Thus, analogously to the stroke therapy described herein, treatment of VEGFD deficiency with VEGFD peptide mimetics may also be beneficial in chronic neurodegenerative diseases by stabilizing neuronal structures, preserving synaptic connectivity, and strengthening neuronal survival.

Materials and Methods

Additional information on the study methodology is provided in *SI Appendix*.

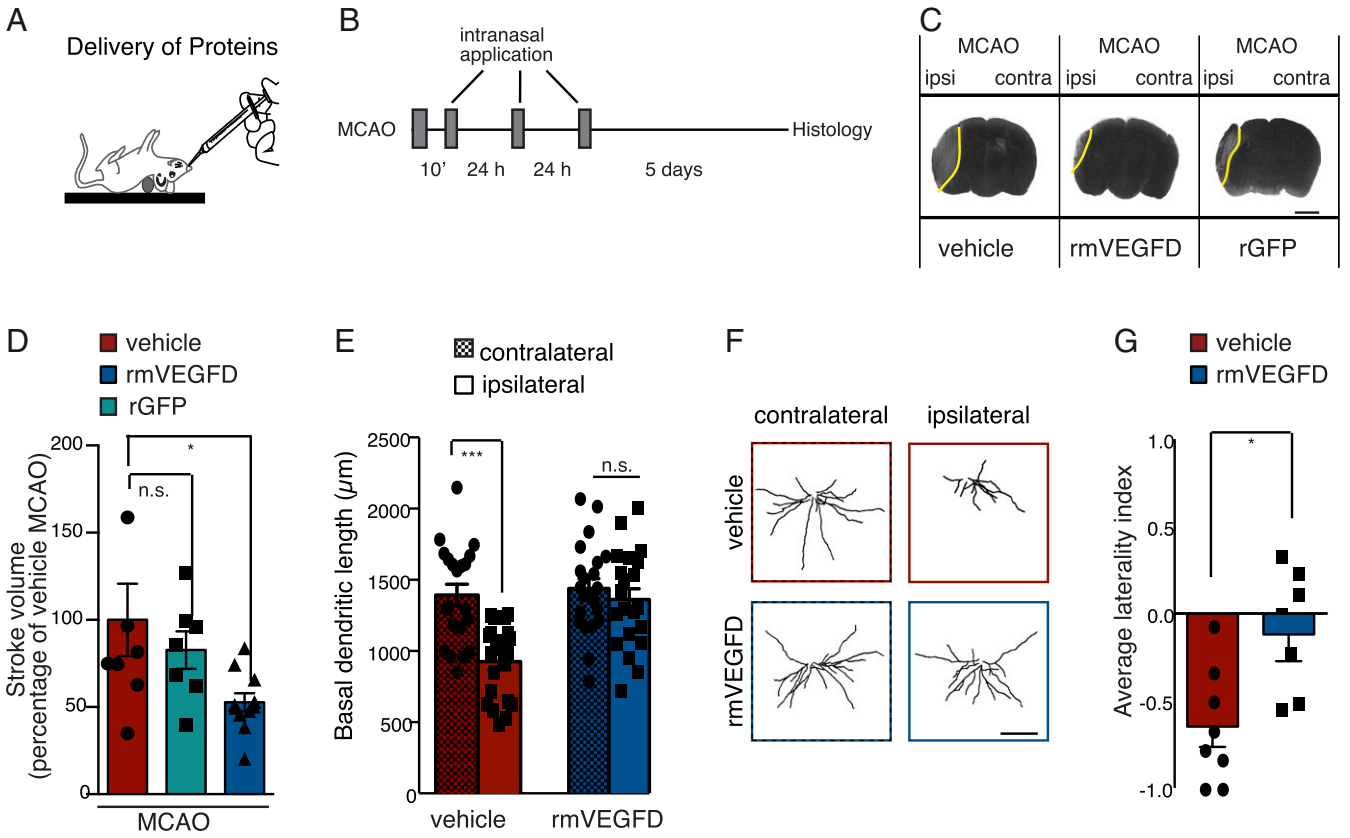

Fig. 3. Nose-to-brain delivery of rmVEGFD prevents MCAO-induced dendrite loss and reduces brain damage. (*A*) Schematic illustration of intranasal protein application. (*B*) Timeframe of the experiment. Recombinant proteins were delivered at 10 min after MCAO to the left naris. Application was repeated at 24 h and 48 h post-MCAO. Histology was performed at 8 d post-MCAO. (*C*) Silver-stained coronal brain sections of mice after MCAO that received nose drops of rmVEGFD, rGFP, or vehicle. (Scale bar: 0.20 cm.) (*D*) Infarct volumes in brains of mice that were subjected to MCAO and received nose drops of rmVEGFD (n = 11), rGFP (n = 7), or vehicle (n = 8). (*E*) Length of the basal dendritic trees of layer 2/3 pyramidal neurons from the ipsilateral and contralateral cortices of mice after MCAO that received nose drops of rmVEGFD or vehicle (n = 21 neurons; 4 mice per condition). (*F*) Representative tracings of layer 2/3 pyramidal neurons as in *E*. (Scale bar: 50 μm.) (*G*) Average laterality index from corner test behavior of mice before and after MCAO that received nose drops of rmVEGFD (n = 7) or vehicle (n = 8). *D*, one-way ANOVA with Dunnett's correction for multiple comparisons; *E*, unpaired *t* test and two-way ANOVA with Bonferroni's correction for multiple comparisons; *G*, unpaired *t* test. *P < 0.05; ***P < 0.001. Plotted data show mean ± SEM and individual values.

Hippocampal Cultures and Treatments. Hippocampal neurons from newborn C57BL/6N mice were isolated and cultured as described previously (8). Pharmacologic treatment was provided using the following drugs: bicuculline (50 μM), NMDA (20 μM, if not indicated otherwise), MK-801 (2 μM), actinomycin D (10 μg/mL), TTX (1 μM), 4AP (250 μM), and rmVEGFD (100 ng/mL).

In Vitro Death Assays and Measurement of Dendritic Damage. Transfection of a plasmid containing an expression vector for hrGFP to visualize in vitro dendritic morphology was performed on day in vitro (DIV) 8 as described previously (6). At DIV10, cultures were either treated with 20 μM NMDA for 10 min or exposed to OGD and then returned to normal conditions and fixed for analysis after 24 h. Neuronal death was assessed by observing the shape of neuronal nuclei and expressed as percentage of dead cells over the total number of neurons analyzed. For morphometric analyses, fluorescence images were acquired using a confocal laser-scanning microscope (TCS SP2; Leica). Total dendritic length was calculated using Fiji software and the Simple Neurite Tracer plugin.

qRT-PCR. Total RNA was extracted from cultures or tissue using the RNeasy Mini Kit (Qiagen) with additional on-column DNase I digestion to eliminate genomic DNA contamination. The extracted RNA was reverse-transcribed into first-strand cDNA using the High-Capacity cDNA Reverse- Transcription Kit (Applied Biosystems). Quantitative reverse transcriptase PCR (qRT-PCR) was performed with a sequence detection system model 7300 Real-Time PCR System using TaqMan Gene Expression Master Mix (Applied Biosystems) and FAM dye-labeled probe sets designed by Applied Biosystems. The expression levels of target genes were normalized to the expression of *Gusb*.

Immunohistochemistry. Coronal brain sections were immunostained directly on microscope slides. Heat-induced epitope retrieval was performed before blocking by incubating the slides in preheated sodium citrate buffer (10 mM sodium citrate and 0.05% Tween 20, pH 6.0) at 95 °C for 10 min. Slides were then incubated in 0.5% Triton-X100 and 10% FCS in PBS for 1.5 h at room temperature. Primary antibodies were diluted in blocking solution and incubated overnight at 4 °C in a humidified chamber. Mouse anti-VEGFD antibody was used (1:100; sc-373866, Santa Cruz Biotechnology), Nuclei were labeled with Hoechst (1:6,000 in PBS; Serva Electrophoresis) for 10 min.

Golgi Staining for In Vivo Analysis of Dendritic Morphology. Golgi impregnation was performed using Rapid Golgi Stain Kit (FD Neuro Technologies) according to the manufacturer's protocol and as described previously (6, 7, 37). Brains were sectioned into 100-μm-thick coronal slices. Z-stacks of Golgi-stained layer 2/3 pyramidal cortical neurons were acquired with a 20× objective mounted on a Nikon Eclipse 90i upright automated microscope at 5-μm intervals. The Simple Neurite Tracer plugin available within the Fiji software was used for quantification.

MCAO and Infarct Size. Permanent MCAO was produced as described previously (21). Mice were anesthetized with 150 μL of 2.5% tribromoethanol per 10 g of body weight. They were allowed to breathe spontaneously and were not ventilated. They were placed supine on a heating pad, a rectal probe was inserted, and body temperature was monitored and maintained between 36.5 and 37.5 °C using a World Precision Instruments ATC 1000 DC temperature controller. The surgical site was disinfected with Braunol (Braun). Under a stereo dissecting microscope (Leica M651), a 1-cm-long midline incision was made between the left eye and the ear. The temporal

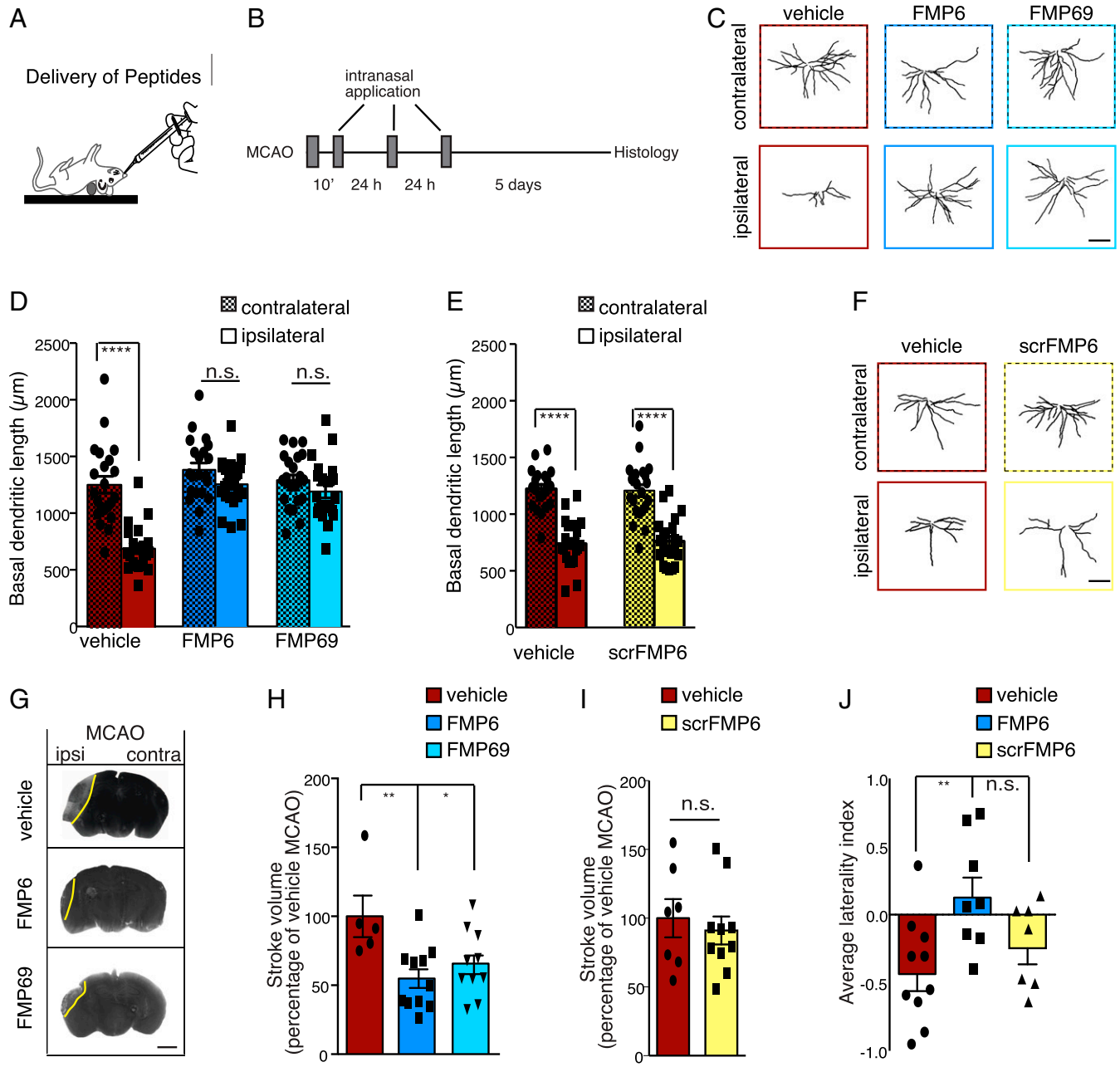

Fig. 4. Nose-to-brain delivery of VEGFD peptide mimetics prevents MCAO-induced dendrite loss and reduces brain damage. (*A*) Schematic illustration of intranasal peptide application. (*B*) Time frame of the experiment. Peptides were delivered at 10 min after MCAO to the left naris. Application was repeated at 24 h and 48 h post-MCAO. Histology was performed at 8 d post-MCAO. (*C*) Representative tracings of the basal dendritic trees of layer 2/3 pyramidal neurons from the ipsilateral and contralateral cortices of mice after MCAO that received nose drops of FMP6, FMP69, or vehicle. (Scale bar: 50 μm.) (*D*) Basal dendritic length of layer 2/3 pyramidal neurons from the ipsilateral and contralateral cortices of mice as in *C* (vehicle: $n = 21$ to 22 neurons, 4 mice; FMP6: $n = 21$ to 22 neurons; 4 mice; FMP69: $n = 21$ to 23 neurons, 4 mice). (*E*) Basal dendritic length of layer 2/3 pyramidal neurons from the ipsilateral and contralateral cortices of mice after MCAO that received nose drops of scrambled peptide (scrFMP6) or vehicle (vehicle: $n = 20$ to 21 neurons, 4 mice; scrFMP6: $n = 22$ neurons, 4 mice). (*F*) Representative tracings of the basal dendritic trees of layer 2/3 Golgi-stained pyramidal neurons as in *E*. (Scale bar: 50 μm.) (*G*) Silver-stained coronal brain sections of mice after MCAO that received nose drops of FMP6, FMP69, or vehicle. (Scale bar: 0.20 cm.) (*H*) Infarct volumes in brains of mice that were subjected to MCAO and received nose drops of FMP6 ($n = 11$), FMP69 ($n = 10$), or vehicle ($n = 5$). (*I*) Infarct volumes in brains of mice that were subjected to MCAO and received nose drops of scrFMP6 ($n = 10$) or vehicle ($n = 7$). (*J*) Average laterality index from corner test behavior of mice before and after MCAO that received nose drops of FMP6 ($n = 8$), scrFMP6 ($n = 7$), or vehicle ($n = 10$). *D* and *E*, unpaired *t* test and two-way ANOVA with Bonferroni's correction for multiple comparisons; *H* and *J*, one-way ANOVA with Dunnett's correction for multiple comparisons; *I*, unpaired *t* test $^*P < 0.05$; $^{**}P < 0.01$; $^{***}P < 0.001$. Plotted data show mean ± SEM and individual values.

muscle was removed by electrocoagulation, and the left middle cerebral artery (MCA) was visible through the semitranslucent temporal surface of the skull. After a small burr hole was made in the temporal bone with a fine drill (Dremel 3000, with flexible extension [Dremel, 225] and diamond cutter [Dremel, 7103]), the inner layer of the skull was removed with fine forceps (Dumont, 55), and the dura mater was carefully opened to expose the left MCA. Care was taken to avoid damage to the brain tissue. 0.9% NaCl was present in the area surrounding the MCA. An Erbe ICC 50 microbipolar electrocoagulator with a bipolar forceps (Erbe 20195-013) was used to permanently occlude the left MCA.

The incision was sutured, and the mice were placed in a 37 °C nursing box to recover from anesthesia, then returned to their home cages. Sham-operated mice were subjected to identical procedures without MCAO. On day 8 after MCAO or sham surgery, animals were killed under deep anesthesia with 400 mg/kg body weight of Narcoren and perfused intracardially with 20 mL of normal saline. The brains were removed from the skull and immediately frozen on dry ice. Eight consecutive 20-μm-thick coronal cryosections were cut every 400 μm and subjected to further histological analysis and determination of total infarct volume using a silver staining technique (21, 38). A total of 20 slices were collected for each brain and analyzed for stroke volume. Stroke volume was expressed relative to the average stroke volume of the vehicle/artificial cerebrospinal fluid (aCSF) MCAO mice in the same experiment. The mean stroke volume observed after MCAO in the vehicle/aCSF MCAO mice used in this study was 17.20 ± 7.39 mm^3.

Intracerebroventricular Delivery. Solutions were delivered by stereotactic injection into the left ventricle of mice that underwent MCAO surgery. For stereotactic injection, mice were still under anesthesia from the MCAO treatment. The fur on the skull was shaved, and the surgical site was disinfected using Braunol (Braun). The animal was then placed in the stereotaxic apparatus (World Precision Instruments). A rectal probe was inserted, and body temperature was monitored and maintained between 36.5 and 37.5 °C using a World Precision Instruments ATC 1000 DC temperature controller. A total volume of 2 μL was injected unilaterally at the following coordinates relative to bregma: anteroposterior, +0.1 mm; mediolateral, +0.9 mm; dorsoventral, −3.0 mm from the skull surface. A total volume of 2.0 μL was injected into the left ventricle at a speed of 400 nL/min. After stereotactic injection, the incision was sutured and the mice was placed in a 37 °C nursing box to recover from anesthesia, then returned to their home cages. Sham-operated mice were subjected to identical procedures with delivery of vehicles. Doses of 200 ng of recombinant proteins (rmVEGFD, R&D Systems; rmVEGFC, Biovision; rmVEGF165, Biovision; GFP, Abcam) were delivered.

Corner Test. Sensorimotor function was assessed using the corner test at 1 d before surgery (day 0) and 1, 3, 4, and 7 d after surgery for mice receiving i.c.v. administration. Mice receiving nose drops were scored at 1 d before MCAO and 3, 4, and 7 d after surgery. A mouse cage without bedding was placed into a black arena (50 cm × 50 cm × 50 cm). Two cardboards were attached on one side at an angle of 30° and were in direct contact with the mouse cage on each side, so that mice remained inside the cardboards. The two cardboards were wrapped with foil to allow easier cleaning after each trial. When facing the 30° angle, mice rear on their hind limbs and turn to either the right or left side. Only turns in which mice fully rose on their hind limbs and made a complete turn were counted. Before the first test session, mice were habituated to the box without cardboards for 5 min. Test sessions were stopped for each mouse if either of the following two criteria were met: a total of 12 complete turns were counted or three trials of 5 min with an intertrial interval of a minimum of 10 min were completed. Daily sessions in which the mice made three or fewer full turns were excluded from the analysis.

The laterality index (LI) was calculated using the following formula: LI = (turns to the left side − turns to the right side)/total number of turns. A negative LI denotes turning to the right side and indicates damage to the left hemisphere (39). Due to drowsiness of the animals following anesthesia, the protocol for the corner test after nasal application of compounds (which required anesthesia) had to be modified to behavioral assessments on days 3, 4, and 7 post-MCAO. In addition, in the mice receiving nose drops, a single average LI value was computed as the average of the deviations from baseline measured on days 3, 4, and 7.

Immunoblotting and Antibody Information. Tissue lysates were prepared in RIPA buffer containing 1% protease inhibitor mixture (Sigma-Aldrich). Protein concentrations in the lysates were estimated by a Bio-Rad protein assay. Lysates were analyzed by standard immunoblot analysis. Samples were separated by 15% sodium dodecyl sulfate-polyacrylamide gel electrophoresis and transferred onto nitrocellulose membranes. Membranes were blocked with 5% milk/phosphate-buffered saline with Tween (PBST) and probed in goat anti-VEGFD antibody and rabbit anti-GFP antibody diluted in 5% BSA/PBST. Mouse anti-tubulin was used as a protein loading control. Membranes were developed with ECL Western blotting detection reagents (Amersham) after incubation with horseradish peroxidase (HRP)-conjugated HRP secondary antibodies: goat anti-VEGFD antibody (R&D Systems; AF469, lot N CM00312091); rabbit anti-GFP antibody (Molecular Probes; A6455); mouse anti-tubulin (Sigma Aldrich; T9026); HRP-conjugated donkey anti-goat IgG (Dianova; 705-035-147, lot N 118345); HRP-conjugated goat anti-rabbit IgG (Dianova; 111-035-144, lot N 94406); and HRP-conjugated goat anti-mouse IgG (Dianova; 715-035-150, lot N 85097).

VEGFD Peptide Mimetics. By systematically diversifying the central helix of VEGFD, a library of 16-aa-long peptides was generated, and the components were tested for their ability to mimic the biological effects of rmVEGFD on neurons. Details are provided in *SI Appendix*. The most potent VEGFD peptide mimetics used for the in vivo part of this study were FMP6 (ALALKEIDEEWQRKGI) and FMP69 (ALTLKE(aib)DEEWQRKGI). The sequence of the scrambled control scrFMP6 was KEWLQALGIKDERAEI. Peptides were synthesized by Metabion with purity >95%; all peptides contain an amide and an acetyl group at the carboxy and amino termini, respectively.

Nose Delivery of Proteins and Peptides. Mice were either still under anesthesia from the MCAO treatment or were mildly anesthetized with <50 μL of 2.5% tribromethanol per 10 g of body weight. Mice were placed in a supine position, and a cotton pad was inserted under the dorsal neck to extend the head back toward the supporting surface. During intranasal application procedures, rectal temperature was maintained at 37 ± 0.5 °C with a World Precision Instruments ATC 1000 DC temperature controller. The indicated concentrations of the intranasal solutions were adjusted with 0.25% of the absorption enhancer tetradecyl-β-D-maltoside (TDM) (40) (Sigma-Aldrich) to a total volume of 20 μL. Recombinant proteins or peptides were delivered in 2-μL drops to the left naris every 2 min over a period of 20 min (20 μL total delivered) using an Eppendorf pipette with a 10-μL filter tip (Nerbe Plus). Mice remained anesthetized for an additional 20 min in the same position. Brains were harvested for immunohistochemistry, Golgi staining, or infarct volume analysis. RmVEGFD (1 μg; R&D Systems) or 1 μg of GFP were delivered in 20 μL of 0.25% TDM for each scheduled delivery; 77 pmol (equivalent to 1 μg of rmVEGFD) of FMP6, FMP69, or scrFMP6 were delivered in 20 μL of 0.25% TDM for each scheduled delivery.

Animals. P0 C57BL/6N mice were used for primary neuronal cultures. For all in vivo experiments, 8-wk-old C57BL/6N SPF male mice weighing 24 to 26 g (Charles River Laboratories) were used. Mice were housed in groups of no more than three in the animal facility at Heidelberg University in standard cages (15 cm × 21 cm × 13.5 cm) on a normal 12:12-h light:dark cycle with ad libitum access to water and food. Each cage contained nesting material. At the start of the experiments, mice weighed 25 ± 1 g. Animals were randomly allocated to treatment groups.

Study Approval. The study was carried out in accordance with national guidelines for the use of experimental animals. The protocols were approved by the governmental committees (Animal Care Committee, Regierungspräsidium Karlsruhe, Referat 35, Karlsruhe, Germany; G-173/13).

Statistics. Plotted data show mean ± SEM and individual values. For in vitro experiments (mortality, qRT-PCR), *N* represents the number of independent preparations of hippocampal cultured neurons. For in vitro experiments (morphology), *N* represents the number of neurons analyzed in each experimental condition; the number of independent preparations of hippocampal cultured neurons is in brackets. For in vivo morphological experiments, *N* represents the number of neurons analyzed in each experimental condition; the number of mice used for each condition is also indicated. For in vivo qRT-PCR experiments, the corner test, and in vivo analysis of infarct size, *N* represents the number of mice used for each condition. The same mice were used to calculate contralateral and ipsilateral values. Animals or dishes were assigned at random to the different experimental groups. In all tests, the experimenter was blinded to the identity of the samples being analyzed. Mice that died after MCAO surgery before the scheduled endpoint were excluded from the analysis; the typical mortality rate was 10 to 20%. All of the surviving mice were included. For the corner test, mice that made three or fewer full turns were excluded from the analysis. *N* values and statistical tests used are indicated in the respective figure legends.

Data Availability Statement. All data shown in the paper are available to readers at Figshare, https://doi.org/10.6084/m9.figshare.11920116.

ACKNOWLEDGMENTS. We thank Iris Bünzli-Ehret for her help with the preparation of hippocampal cultures and Dr. Anna M. Hagenston for her advice on astrocytic primary cultures. We also thank Netta Ussyshkin for technical help, Dr. Thomas Bruckner (Medical Biometry and Computer Science, Heidelberg University) for help with statistical analyses, and Michael Wacker for his help with the synthesis of the VEGFD peptide mimetics library. All images of Golgi-impregnated

tissues were obtained at the Nikon Imaging Center at Heidelberg University. This work was supported by the Deutsche Forschungsgemeinschaft (BA 1007/4-1), the European Research Council (Proof of Concept-2014_640892_VEGFDANI), Forschergruppe FOR2325, and the Sonderforschungsbereich (SFB 1158). H.B., C.D.K., and D.M. are members of the Excellence Cluster *CellNetworks* at Heidelberg University.

1. E. J. Benjamin *et al*.; American Heart Association Council on Epidemiology and Prevention Statistics Committee and Stroke Statistics Subcommittee, Heart disease and stroke statistics—2019 update: A report from the American Heart Association. *Circulation* **139**, e56–e528 (2019).
2. A. Moussaddy, A. M. Demchuk, M. D. Hill, Thrombolytic therapies for ischemic stroke: Triumphs and future challenges. *Neuropharmacology* **134**, 272–279 (2018).
3. A. J. Koleske, Molecular mechanisms of dendrite stability. *Nat. Rev. Neurosci.* **14**, 536–550 (2013).
4. C. E. Brown, P. Li, J. D. Boyd, K. R. Delaney, T. H. Murphy, Extensive turnover of dendritic spines and vascular remodeling in cortical tissues recovering from stroke. *J. Neurosci.* **27**, 4101–4109 (2007).
5. C. L. Gonzalez, B. Kolb, A comparison of different models of stroke on behaviour and brain morphology. *Eur. J. Neurosci.* **18**, 1950–1962 (2003).
6. D. Mauceri, H. E. Freitag, A. M. Oliveira, C. P. Bengtson, H. Bading, Nuclear calcium-VEGFD signaling controls maintenance of dendrite arborization necessary for memory formation. *Neuron* **71**, 117–130 (2011).
7. T. J. Hemstedt, C. P. Bengtson, O. Ramírez, A. M. M. Oliveira, H. Bading, Reciprocal interaction of dendrite geometry and nuclear calcium-VEGFD signaling gates memory consolidation and extinction. *J. Neurosci.* **37**, 6946–6955 (2017).
8. D. Mauceri, A. M. Hagenston, K. Schramm, U. Weiss, H. Bading, Nuclear calcium buffering capacity shapes neuronal architecture. *J. Biol. Chem.* **290**, 23039–23049 (2015).
9. C. Litke, H. Bading, D. Mauceri, Histone deacetylase 4 shapes neuronal morphology via a mechanism involving regulation of expression of vascular endothelial growth factor D. *J. Biol. Chem.* **293**, 8196–8207 (2018).
10. S. A. Stacker, M. G. Achen, Emerging roles for VEGF-D in human disease. *Biomolecules* **8**, E1 (2018).
11. M. Uhlén *et al*., Proteomics. Tissue-based map of the human proteome. *Science* **347**, 1260419 (2015).
12. A. Saunders *et al*., Molecular diversity and specializations among the cells of the adult mouse brain. *Cell* **174**, 1015–1030.e16 (2018).
13. A. Zeisel *et al*., Molecular architecture of the mouse nervous system. *Cell* **174**, 999–1014.e22 (2018).
14. G. E. Hardingham, Y. Fukunaga, H. Bading, Extrasynaptic NMDARs oppose synaptic NMDARs by triggering CREB shut-off and cell death pathways. *Nat. Neurosci.* **5**, 405–414 (2002).
15. C. P. Bengtson, O. Dick, H. Bading, A quantitative method to assess extrasynaptic NMDA receptor function in the protective effect of synaptic activity against neurotoxicity. *BMC Neurosci.* **9**, 11 (2008).
16. H. Bading, Therapeutic targeting of the pathological triad of extrasynaptic NMDA receptor signaling in neurodegenerations. *J. Exp. Med.* **214**, 569–578 (2017).
17. S. A. Lipton, Pathologically activated therapeutics for neuroprotection. *Nat. Rev. Neurosci.* **8**, 803–808 (2007).
18. Q. J. Wu, M. Tymianski, Targeting NMDA receptors in stroke: New hope in neuroprotection. *Mol. Brain* **11**, 15 (2018).
19. D. J. Rossi, T. Oshima, D. Attwell, Glutamate release in severe brain ischaemia is mainly by reversed uptake. *Nature* **403**, 316–321 (2000).
20. F. N. Soria *et al*., Extrasynaptic glutamate release through cystine/glutamate antiporter contributes to ischemic damage. *J. Clin. Invest.* **124**, 3645–3655 (2014).
21. S. J. Zhang *et al*., A signaling cascade of nuclear calcium-CREB-ATF3 activated by synaptic NMDA receptors defines a gene repression module that protects against extrasynaptic NMDA receptor-induced neuronal cell death and ischemic brain damage. *J. Neurosci.* **31**, 4978–4990 (2011).
22. B. Buchthal, U. Weiss, H. Bading, Post-injury nose-to-brain delivery of activin A and SerpinB2 reduces brain damage in a mouse stroke model. *Mol. Ther.* **26**, 2357–2365 (2018).
23. Y. J. Shin *et al*., Induction of vascular endothelial growth factor receptor-3 mRNA in glial cells following focal cerebral ischemia in rats. *J. Neuroimmunol.* **229**, 81–90 (2010).
24. D. García-Chávez *et al*., Long-term evaluation of cytoarchitectonic characteristics of prefrontal cortex pyramidal neurons, following global cerebral ischemia and neuroprotective melatonin treatment, in rats. *Neurosci. Lett.* **448**, 148–152 (2008).
25. C. E. Brown, J. D. Boyd, T. H. Murphy, Longitudinal in vivo imaging reveals balanced and branch-specific remodeling of mature cortical pyramidal dendritic arbors after stroke. *J. Cereb. Blood Flow Metab.* **30**, 783–791 (2010).
26. S. J. Zhang *et al*., Nuclear calcium signaling controls expression of a large gene pool: Identification of a gene program for acquired neuroprotection induced by synaptic activity. *PLoS Genet.* **5**, e1000604 (2009).
27. H. Bading, Nuclear calcium signalling in the regulation of brain function. *Nat. Rev. Neurosci.* **14**, 593–608 (2013).
28. S. R. Alcalá-Barraza *et al*., Intranasal delivery of neurotrophic factors BDNF, CNTF, EPO, and NT-4 to the CNS. *J. Drug Target.* **18**, 179–190 (2010).
29. R. G. Thorne, G. J. Pronk, V. Padmanabhan, W. H. Frey, 2nd, Delivery of insulin-like growth factor-I to the rat brain and spinal cord along olfactory and trigeminal pathways following intranasal administration. *Neuroscience* **127**, 481–496 (2004).
30. D. B. Renner *et al*., Intranasal delivery of insulin via the olfactory nerve pathway. *J. Pharm. Pharmacol.* **64**, 1709–1714 (2012).
31. I. D. Neumann, R. Maloumby, D. I. Beiderbeck, M. Lukas, R. Landgraf, Increased brain and plasma oxytocin after nasal and peripheral administration in rats and mice. *Psychoneuroendocrinology* **38**, 1985–1993 (2013).
32. Y. Ozsoy, S. Gungor, E. Cevher, Nasal delivery of high molecular weight drugs. *Molecules* **14**, 3754–3779 (2009).
33. Y. Rodríguez Cruz *et al*., Treatment with nasal neuro-EPO improves the neurological, cognitive, and histological state in a gerbil model of focal ischemia. *ScientificWorldJournal* **10**, 2288–2300 (2010).
34. J. P. Yang *et al*., The dose-effectiveness of intranasal VEGF in treatment of experimental stroke. *Neurosci. Lett.* **461**, 212–216 (2009).
35. J. J. Lochhead, T. P. Davis, Perivascular and perineural pathways involved in brain delivery and distribution of drugs after intranasal administration. *Pharmaceutics* **11**, E598 (2019).
36. V. M. Leppänen *et al*., Structural determinants of vascular endothelial growth factor-D receptor binding and specificity. *Blood* **117**, 1507–1515 (2011).
37. M. Simonetti *et al*., Nuclear calcium signaling in spinal neurons drives a genomic program required for persistent inflammatory pain. *Neuron* **77**, 43–57 (2013).
38. O. Herrmann *et al*., IKK mediates ischemia-induced neuronal death. *Nat. Med.* **11**, 1322–1329 (2005).
39. J. Lubjuhn *et al*., Functional testing in a mouse stroke model induced by occlusion of the distal middle cerebral artery. *J. Neurosci. Methods* **184**, 95–103 (2009).
40. J. J. Arnold, F. Ahsan, E. Meezan, D. J. Pillion, Correlation of tetradecylmaltoside induced increases in nasal peptide drug delivery with morphological changes in nasal epithelial cells. *J. Pharm. Sci.* **93**, 2205–2213 (2004).